Three-Dimensional Coherent X-Ray Diffraction Microscopy

Ian K. Robinson and Jianwei Miao

Abstract

X-rays have been widely used in the structural analysis of materials because of their significant penetration ability, at least on the length scale of the granularity of most materials. This allows, in principle, for fully three-dimensional characterization of the bulk properties of a material. One of the main advantages of x-ray diffraction over electron microscopy is that destructive sample preparation to create thin sections is often avoidable. A major disadvantage of x-ray diffraction with respect to electron microscopy is its inability to produce real-space images of the materials under investigation—there are simply no suitable lenses available. There has been significant progress in x-ray microscopy associated with the development of lenses, usually based on zone plates, Kirkpatrick–Baez mirrors, or compound refractive lenses. These technologies are far behind the development of electron optics, particularly for the large magnification ratios needed to attain high resolution. In this article, the authors report progress toward the development of an alternative general approach to imaging, the direct inversion of diffraction patterns by computation methods. By avoiding the use of an objective lens altogether, the technique is free from aberrations that limit the resolution, and it can be highly efficient with respect to radiation damage of the samples. It can take full advantage of the three-dimensional capability that comes from the x-ray penetration. The inversion step employs computational methods based on oversampling to obtain a general solution of the diffraction phase problem.

Keywords: *microscopy, nanocrystal shapes, strain, three-dimensional coherent x-ray diffraction.*

Introduction

The development of a fully three-dimensional (3D) x-ray diffraction microscopy method would revolutionize materials science because it would allow routine characterization of all granular materials. Most hard materials have crystalline grains, whose boundary interactions are responsible for most of the mechanical, electrical, and thermodynamic properties. The ability to visualize the distribution of strains within each grain at atomic resolution in three dimensions while these interactions are taking place *in situ* must come close to the ideal method of materials analysis. A short list of materials challenges that might be addressed includes quantum dot and wire structures, dislocation structure and dynamics, ion-beam interactions, deformation structures, crystal growth, and coarsening kinetics. At the end of this article, we will discuss the possibility of single-molecule imaging that would be enabled by the development of new x-ray sources.

Background

The basic requirement for a coherent diffraction experiment is to prepare and then illuminate the sample with a spatially coherent beam of x-rays, meaning that the transverse coherence length should exceed the dimensions of the sample. The coherence length is determined by the divergence (or convergence) and the bandwidth of the incident x-ray beam. Under these conditions, scattering from all parts of the sample can be expected to interfere in the far-field diffraction pattern. Coherent x-ray diffraction (CXD) effects were observed by Yun et al.[1] in 1987 and by Sutton et al.[2] in 1990. CXD is usually measured with a CCD x-ray detector positioned far enough away that all the fine fringes can be resolved. As will be discussed in more detail later, this also assures the required oversampling of the diffraction pattern. Two versions of such experiments are compared in this review, with relative advantages and disadvantages: the first is based on forward x-ray diffraction, while the second employs Bragg diffraction from the sample's crystal planes. In order for the forward x-ray diffraction experiment to work, great care must be taken in placing guard slits around the incident beam, while for the Bragg experiment, an additional coherence constraint applies: the longitudinal coherence must exceed the longest optical-path length difference of rays traversing the sample.

When a coherent beam of x-rays illuminates a small crystalline or noncrystalline sample, the far-field diffraction intensities are continuous and weak. This continuous diffraction pattern can hence be sampled at a spacing finer than the Bragg peak (spatial) frequency (i.e., oversampled). The Bragg peak frequency is defined as the inverse of the sample size. It was first suggested by Sayre[3] in 1952 that having additional measurements of the Fourier magnitudes for a crystal *between* the Bragg peaks might provide phase information. Based on the argument that the electron density autocorrelation function of an object is twice as large as the object itself, Bates[4] concluded in 1982 that retrieval of the phases from the diffraction intensities required 2× finer oversampling of the intensities than the Bragg peak frequency in each dimension. Millane[5] in 1996 generalized Bates' criterion to three dimensions (and higher). In 1998, Miao et al.[6] proposed a different justification of oversampling and concluded that both Bates' and Millane's criteria were overly restrictive. A sufficient criterion was that the product of the oversampling ratios (σ, the density of measurement points divided by Bragg density) in all spatial dimensions, $\sigma_x\sigma_y\sigma_z$, should be greater than 2. This explanation has so far been consistent with both computer simulations and experimental results.[6,7]

To understand why oversampling can provide phase information, consider each intensity point as representing a nonlinear

equation, related to the electron density of the sample by the square of the magnitude of the Fourier transform. The experiment measures the amplitude of the Fourier transform of the electron density, but cannot measure the phase, which is needed to invert the data back to an image. The solution of this so-called phase problem becomes the recovery of a set of unknown variables, the electron density points, from a number of independent equations representing the intensity measurements, ignoring any crystallographic symmetry. When the diffraction pattern is sampled at the Bragg peak frequency, there are exactly twice as many unknown variables as the number of equations,[8] which is why the phases cannot be directly recovered without additional constraints. If the diffraction pattern is oversampled, the number of equations increases, while the number of unknown variables remains the same. When there are more equations (assuming independence) than unknown variables, unique phase information is embedded within the diffraction magnitudes. Oversampling a diffraction pattern in reciprocal space corresponds to surrounding the electron density of the sample in real space with an empty, no-density region,[8] which increases in size with the oversampling ratio (σ), which is also the total volume of the electron density and zero-density regions divided by the electron density region alone.[6] When $\sigma > 2$, the number of equations is greater than unknown variables and the phases can be determined, in principle.

It should be emphasized again that experiments that depend upon oversampling require at least 2× better coherence of the incident x-rays than the Bragg frequency sampling cases because finer features have to be recorded in the diffraction patterns.[9] Having a greater number of equations than unknown variables is a necessity but is not a guarantee of a unique solution. By using the theory of polynomials, it has been shown that while there are a limited number of multiple solutions for 1D objects, multiple solutions are rare for 2D and 3D objects.[10] This statement applies to complete and perfectly accurate data; the situation with real data requires testing, case by case, with experiments.

Oversampling a 2D or 3D diffraction pattern with $\sigma > 2$ can make the phases unique, but no analytic solution has so far been developed to extract the unique phases from a large number of nonlinear equations. The most effective way at the moment is to use iterative algorithms, which Fienup[11] developed in 1978 by enhancing the method of Gerchberg and Saxton.[12] The algorithms iterate back and forth between real and reciprocal space, where constraints are enforced on each iteration. The algorithms were further developed in subsequent years and have now reached a point that the phases can be reliably recovered from oversampled diffraction data, even in the presence of significant noise. Each iteration of the algorithm generally consists of the following four steps: (1) A complex reciprocal-space array is constructed from the current phase set and the square root of the measured diffraction intensity on a suitable grid. For the initial cycle, a random phase set is used. (2) By applying the fast Fourier transform, an electron density distribution on a second grid is calculated from the reciprocal space array. (3) A "support constraint" is applied to separate the electron density from the no-density region. The electron density outside the support and the negative electron density inside the support are pushed close to zero. (4) A new reciprocal-space array is calculated by applying the inverse fast Fourier transform to the new electron density. The phases of the new reciprocal-space array are then adopted in the next iteration after setting the phase of the central pixel to zero. The shape of the support, which is clearly fundamental to the method, has to be known reliably from external sources or may have to be "learned" as the algorithm proceeds.[13]

Imaging Nanopatterned Nickel

The first experimental demonstration of x-ray diffraction microscopy using the oversampling method and an iterative algorithm was carried out by Miao et al.[14] in 1999 to retrieve the phases for a diffraction pattern of a noncrystalline sample. Since then, the method has been successfully applied to image a variety of noncrystalline samples and nanocrystals. These include recent 2D reconstructions using soft x-ray CXD at the Advanced Light Source[13,15] in addition to the three-dimensional CXD imaging[7,9] discussed in this article. Figure 1 shows the forward CXD pattern recorded from a double-layered sample, fabricated in Ni by electron-beam lithography on a Si_3N_4 membrane.[9] The two layers of the pattern have the same structure but were separated by a 1-μm-thick polymer film and rotated 65° relative to each other. A scanning electron microscope (SEM) image of the sample (Figure 2a) shows the top pattern, but the bottom one is blurred. The CXD experiment was performed on an undulator beamline at the Japanese synchrotron facility SPring-8. The phases were retrieved from the oversampled intensities using the iterative algorithm, as shown in Figure 2b.[9] The resolution of the image is ~8 nm, as determined by the upper range cutoff of the diffraction pattern. Due to the longer penetration length of x-rays, compared with electrons, both the top and bottom patterns in the sample

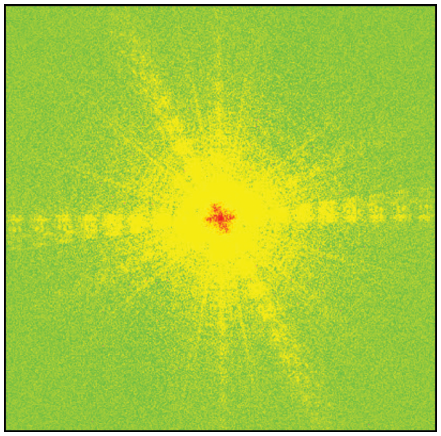

Figure 1. A high-resolution diffraction pattern recorded from a fabricated Ni sample, displayed using a logarithmic scale.

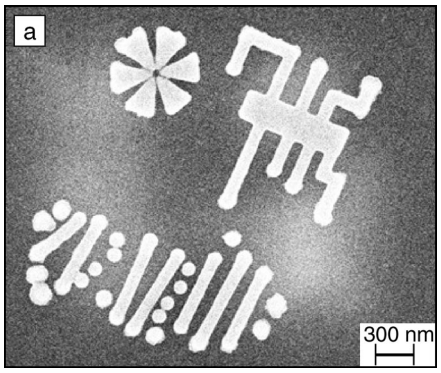

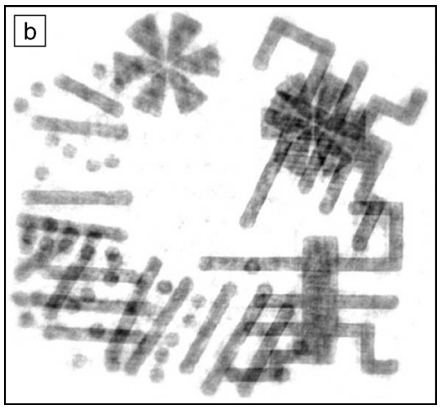

Figure 2. (a) Scanning electron microscopy (SEM) image of the double-layered Ni sample used in Figure 1. The top pattern is visible, but the bottom pattern is blurred. (b) X-ray image reconstructed from Figure 1 with a resolution of ~8 nm; top and bottom patterns are both visible.

are clearly visible. More electron density variation on a nanometer scale is visible in the x-ray image than in the SEM image. To obtain the 3D structure of the sample, a total of 31 2D diffraction patterns were recorded by rotating the sample from –75° to +75° in 5° increments; the total data acquisition time was about 20 h. By using a 3D reconstruction algorithm, the 3D structure of the sample was successfully reconstructed from a set of 2D patterns.[9] Figure 3 shows an iso-surface rendering of the reconstructed 3D structure. The finest division along the vertical axis corresponds to 25 nm, and the distance between two patterns is ~1 μm, which is consistent with the known sample construction.

Imaging Crystalline Structures

We now turn to the application of Bragg diffraction imaging methods to the study of crystalline materials. The crystal lattice introduces a powerful new constraint on the selection of a grain for imaging. A polycrystalline sample will have closely packed grains with many different orientations. Bragg diffraction from this kind of sample will resemble that of a powder, but with a small enough beam (~30 μm across) and typical grain sizes of around a micrometer, the individual grains can still be separated. Even highly textured samples still have enough distribution of orientations that the grains can usually be distinguished. Once a Bragg peak is isolated and aligned, its internal intensity distribution can be recorded by means of a CCD detector at the end of a long detector arm. Figure 4 shows the Ewald construction of the 2D section of the 3D diffraction pattern generated on the CCD for a certain angle near the center of the Bragg peak of the sample. When the sample is rotated through a series of closely spaced angles, 3D data are generated in sections, as illustrated. For a sample ~1 μm in size, only small rotations of the sample through a fraction of a degree are necessary to record a complete 3D data set for the corresponding Bragg reflection. The average intensity decays rapidly away from the center, eventually reaching the background level of the detector. This radial cutoff determines the spatial resolution of the resulting inverted image. This is limited in practice by the counting statistics, but more practically by the stability of the sample and instrument, as well as by the brightness of the x-ray source. At present, the typical resolution of the Bragg diffraction CXD experiments is around 70 nm.

For an ideal crystal, meaning that its unit cells lie on a perfect 3D mathematical lattice, this distribution is the same around every Bragg peak and, indeed, about the origin of reciprocal space. In this case, the Bragg CXD experiment measures the same thing as the forward-scattering CXD experiment, with the important exception that all of the structure around the direct beam (due to window, air, or slit scatter, for example) can be eliminated. This argument also implies that the diffraction should be locally symmetric about the center of each Bragg reflection, resulting in symmetric intensity patterns in the CCD. This is sometimes but not always observed. When a nonsymmetric pattern is seen, it can be decomposed into symmetric and asymmetric parts. For an ideal crystal, the symmetric part can be considered as coming from the real part of the electron density, while the asymmetric part is associated with an imaginary density that may represent a

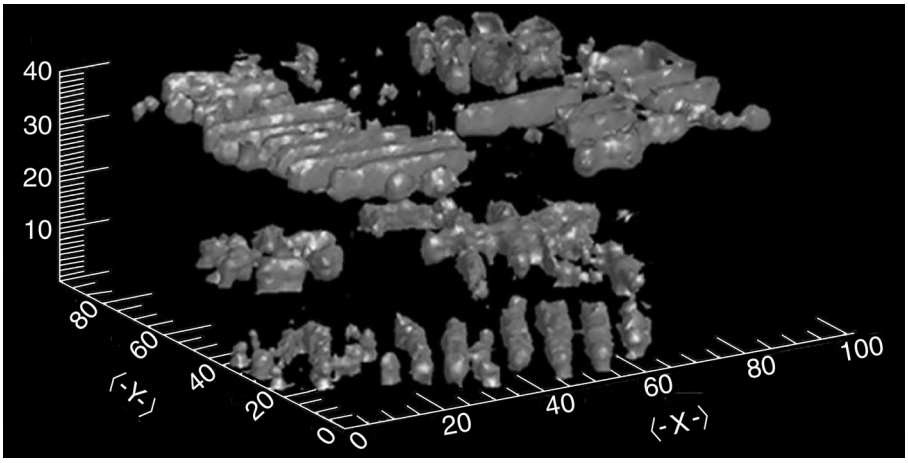

Figure 3. Reconstructed three-dimensional (3D) structure of the Ni sample in Figure 1 displayed in iso-surface rendering. The fine divisions on the vertical axis are 25 nm each; the x and y axes are in nm.

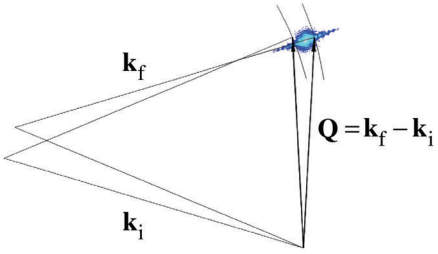

Figure 4. Ewald construction showing how small tilts of the sample cause the detector plane to sweep through the 3D diffraction pattern. The difference between the incident and exit x-ray wave vectors, denoted $\mathbf{k}_i$ and $\mathbf{k}_f$, determines the momentum transfer, $\mathbf{Q}$.

component of strain projected onto the Bragg peak in use.[16] Although they have not yet been demonstrated experimentally, important materials science applications involving local microstructure and defects can be expected in the future from this acute sensitivity to strain.

Imaging Self-Assembled Gold Nanoparticles

A good example of Bragg diffraction CXD is the 3D imaging of nanocrystals of gold.[17] These experiments were carried out at the Advanced Photon Source (APS) using undulator x-rays of 9.5 keV. The use of a Si(333) monochromator reflection ensured sufficient longitudinal coherence. The samples were prepared *in situ* by high-temperature annealing of a thin Au film previously evaporated onto the oxide of a silicon wafer. A 1000 Å film was found to produce oval-shaped nanocrystals about 2 μm long, 1 μm wide, and slightly less than 1 μm thick, with well-developed facets, especially the (111) planes that are parallel to the substrate. A grain was selected from the off-specular $(11\bar{1})$ powder ring and the 3D diffraction pattern was recorded on a 22.5-μm-pixel CCD array located 2.8 m away by rotating the sample in steps of 0.002°.

A typical diffraction pattern at the center of the rocking curve is shown in Figure 5a. This pattern has been symmetrized by averaging with a rotated copy to remove the small effects of strain discussed earlier. The two main fringe patterns are the long modulated diagonal streak, oriented close to the ⟨111⟩ direction of the primary facets, and the concentric ring pattern, typical of any compact object. The size of the sample can be estimated directly from these fringe spacings, which allows us to postulate the "support" to be used as a real-space constraint in the iterative refinement of phases. Alternate cycles of

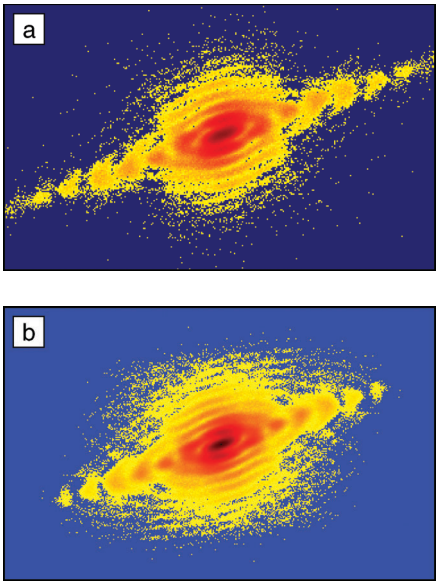

Figure 5. (a) Measured diffraction pattern of a single Au nanocrystal. This pattern, symmetrized to remove the small effects of strain, represents the central slice of a 3D diffraction pattern. (b) Simulated diffraction pattern of the same slice as in (a), from the phased 2D image of the projection of the nanocrystal.

Fienup's hybrid input–output (HIO) and error-reduction[11] algorithms were found to lead to a solution without apparent stagnation of the computation.[11] The diffraction pattern calculated from the final image is shown in Figure 5b. The uniqueness of the solution was demonstrated experimentally by obtaining almost indistinguishable images, starting from different sets of random phase numbers used to "seed" the algorithm.

Several slices from the 3D image of a Au nanocrystal obtained from a full angular series[17] are shown in Figure 6. The first characteristic feature, the bright spot in the central and nearby slices in Figure 6b, was anticipated from earlier experiments and theoretical considerations.[18] A beamline Be window, 6 m in front of the sample, was found to introduce a second component to the mutual intensity function describing the coherence. The second component has a much shorter coherence length, which ultimately determines the size of the bright spot in the image.[18] The second important feature in Figure 6b is that the contrast structure can be seen throughout the interior of the crystal. This mainly appears as stripes, oriented perpendicular to both the ⟨111⟩ and ⟨11$\bar{1}$⟩ directions, but also dark regions where the stripes merge. It is believed that the dark regions are not empty, but filled with Au

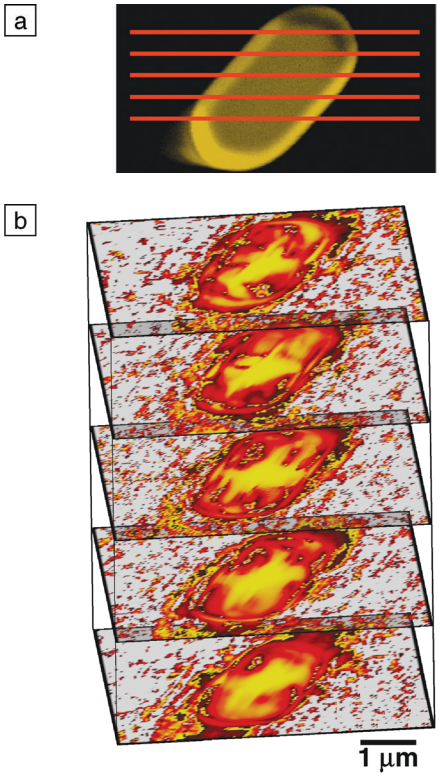

Figure 6. Sections through the real-space 3D image of a typical Au nanocrystal. (a) Schematic illustration of the position of diffraction image sections through a SEM image of the nanocrystal; (b) stacked diffraction images through sections separated by 0.69 μm, as described in Reference 17.

with an orientation that is twinned with respect to the rest of the nanocrystal. Striped slip zones with approximately the observed spacing are known to form along {111} planes in fcc metals during deformation.[19] It is surprising that so much internal structure is visible in a simple isolated metal crystal, grown *in situ* without further processing. This may indicate the presence of considerable residual stress associated with the separation of the grains during their formation.[20]

Potential for Single-Molecule Imaging

Finally, we would like to address the long-term extrapolation of the capabilities of 3D x-ray diffraction microscopy to single-molecule imaging. The oversampling requirement discussed earlier implies that the iterative Fourier transform methods[11,12] will not work in general on crystallographic data. There are too many degrees of freedom for all of the density points in the unit cell of a crystal to be constrained by the amplitude-only data. This is usually called the crystallographic phase problem. However, if a small crystal is used instead, the diffraction extends away from the Bragg points; intensity measurements between the Bragg peaks can provide additional information that can allow a solution of the phase problem. The extreme limit of a single unit cell, for which the diffraction pattern is a smooth continuous function with no Bragg peaks at all, is highly interesting for the study of molecules that do not crystallize readily, such as membrane proteins. Single-molecule imaging has already been demonstrated by electron diffraction from double-walled carbon nanotubes.[21] To avoid radiation damage to the sample, the measurement of the diffraction pattern must be completed before the atomic nuclei and the accompanying core electrons within the molecule become displaced by more than a bond length. This time period, estimated to be around 50 fs,[22] is within the range of accessibility of future x-ray free-electron lasers (XFELs) based on linear particle accelerators. The vital importance of the potential application to solve the structures of proteins is a strong driving force for the construction of XFEL sources in the coming decade.

Acknowledgments

We gratefully acknowledge our respective collaborators, including Keith Hodgson, Tetsuya Ishikawa, Yoshinori Nishino, Mark Pfeifer, Ivan Vartanyants, and Garth Williams. This work was supported by the U.S. National Science Foundation under grant DMR 03-08660 and by the U.S. Department of Energy, Office of Basic Energy Sciences, at Stanford Synchrotron Radiation Laboratory. The use of the Advanced Photon Source beamline 33-ID-D was provided by UNICAT, which is operated by the University of Illinois Materials Research Laboratory and funded by DOE under contract DEFG02-91ER45439, Oak Ridge National Laboratory, the National Institute of Standards and Technologies, and UOP Research & Development. APS is itself supported by the DOE under contract W-31-109-ENG-38. Use of beamline BL29XUL at SPring-8 was supported by RIKEN.

References

1. W-B. Yun, J. Kirz, and D. Sayre, *Acta Crystallogr. A* **43** (1987) p. 131.
2. M. Sutton, S.G.J. Mochrie, T. Greytak, S.E. Nagler, L.E. Berman, G.A. Held, and G.B. Stephenson, *Nature* **352** (1991) p. 608.
3. D. Sayre, *Acta Crystallogr.* **5** (1952) p. 843.
4. R.H.T. Bates, *Optik* **61** (1982) p. 247.
5. R.P. Millane, *J. Opt. Soc. Am. A* **13** (1996) p. 725.
6. J. Miao, D. Sayre, and H.N. Chapman, *J. Opt. Soc. Am. A* **15** (1998) p. 1662.

7. J. Miao, T. Ishikawa, E.H. Anderson, and K.O. Hodgson, *Phys. Rev. B* **67** 174104 (2003).
8. J. Miao and D. Sayre, *Acta Crystallogr. A* **56** (2000) p. 596.
9. J. Miao, T. Ishikawa, B. Johnson, E.H. Anderson, B. Lai, and K.O. Hodgson, *Phys. Rev. Lett.* **89** 088303 (2002).
10. Y.M. Bruck and L.G. Sodin, *Opt. Commun.* **30** (1979) p. 304.
11. J.R. Fienup, *Opt. Lett.* **3** (1978) p. 27.
12. R.W. Gerchberg and W.O. Saxton, *Optik* **35** (1972) p. 237.
13. S. Marchesini, H. He, H.N. Chapman, S.P. Hau-Riege, A. Noy, M.R. Howells, U. Weierstall, and J.C.H. Spence, *Phys. Rev. B* **68** 140101 (2003).
14. J. Miao, P. Charalambous, J. Kirz, and D. Sayre, *Nature* **400** (1999) p. 342.
15. H. He, S. Marchesini, M.R. Howells, U. Weierstall, H.N. Chapman, S. Hau-Riege, A. Noy, and J.C.H. Spence, *Phys. Rev. B* **67** 174114 (2003).
16. I.K. Robinson and I.A. Vartanyants, *Appl. Surf. Sci.* **182** (2001) p. 186.
17. G.J. Williams, M.A. Pfeifer, I.A. Vartanyants, and I.K. Robinson, *Phys. Rev. Lett.* **90** 175501-1 (2003).
18. I.A. Vartanyants and I. K. Robinson, *J. Phys.: Condens. Matter* **13** 10593-611 (2001).
19. H.W. Hayden, W.G. Moffat, and J. Wulff, *Structure and Properties of Materials III* (John Wiley & Sons, New York, 1965).
20. A.H. Cottrell, *The Mechanical Properties of Metals* (John Wiley & Sons, New York, 1964).
21. J.M. Zuo, I. Vartanyants, M. Gao, R. Zhang, and L.A. Nagahara, *Science* **300** (2003) p. 1419.
22. R. Neutze, R. Wouts, D. van der Spoel, E. Weckert, and J. Hajdu, *Nature* **406** (2000) p. 752.
□